

Particle approximation of the two-fluid model for superfluid ^4He using smoothed particle hydrodynamics

Satori Tsuzuki*

Research Center for Advanced Science and Technology,
The University of Tokyo, 4-6-1, Komaba, Meguro-ku, Tokyo 153-8904, Japan
(Dated: March 2020)

This paper presents a finite particle approximation of the two-fluid model for liquid ^4He . We propose the use of smoothed particle hydrodynamics (SPH), a Lagrangian particle method well-established in astrophysics. To solve the equation of motion, we introduce an auxiliary equation that represents a microscopic relationship between entropy and temperature, which derived from quantum statistical mechanics, in elementary particle physics. In numerical simulations, we use a Riemann solver among neighboring particles, as an alternative to artificial viscosity, to stabilize the simulation. We focused on the state of complete phase separation and demonstrate a Rayleigh-Taylor instability simulation, confirming the emergence of the characteristic mushroom structure in the linear growth regime. Furthermore, we investigated the applicability of SPH to entropy wave propagation analyses by examining the effect of density fluctuations on the error of calculations with a benchmark case. The simulation results show good agreement with those of FDM and with the analytical solution. Consequently, our simulation model has been confirmed to reproduce the phenomenological characteristics of superfluid ^4He qualitatively. We have thus pioneered a new paradigm of Lagrangian particle mechanics, which will hopefully stimulate further numerical studies of superfluids in condensed matter physics.

I. INTRODUCTION

The bizarre behavior of liquid helium 4 (hereinafter, ^4He) has attracted the attention of condensed matter physicists for many years; however, the detailed dynamics of this fluid remains a mystery even now, eighty years after its discovery.

Figure 1 reviews the basic properties of ^4He through a schematic phase diagram. In 1937, P. L. Kapitza found that the viscosity of liquid ^4He decreases upon cooling and reaches almost zero below the λ -point (labelled point c in Fig. 1). Liquid ^4He was later confirmed to display viscosity in the high-temperature area over the λ -line, and to lose it in the low-temperature area below the λ -line. Once lack of viscosity is achieved in this latter temperature range, liquid ^4He displays many unexpected properties that characterize it as a “superfluid.” In contrast, liquid ^4He within the high-temperature area over the λ -line is still classified as a “normal fluid.”

The superfluidity condition is characterized by properties such as the following two examples. Superfluid ^4He can penetrate a high-density capillary filter (e.g., GYP-sum), thanks to the so-called “superleak effect”, whereas this is not possible for normal fluid ^4He . In addition, the “film flow effect” takes place when superfluid ^4He spontaneously comes out of its vessel as a result of van der Waals forces between helium atoms and walls being stronger than the forces between ^4He atoms themselves.

Many physicists have made efforts to explain these interesting properties of superfluids at both the ontological and phenomenological level. One year after the discovery by P. L. Kapitza, F.W. London explained the phase transition of liquid ^4He from a quantum mechanical point of

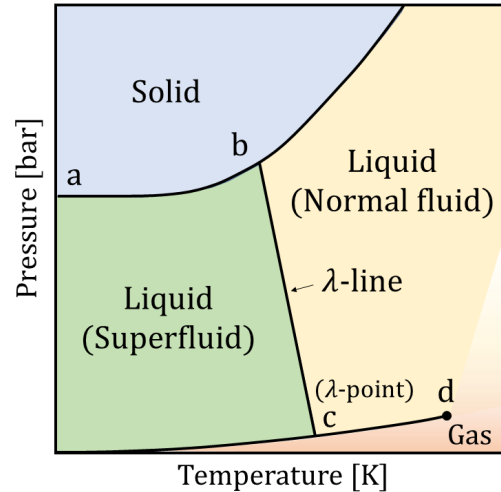


FIG. 1. Schematic phase diagram of ^4He . Points a , b , c , and d correspond to the following (p, T) values, respectively: (25bar, 0K), (30bar, 1.77K), (50.5mbar, 2.17K), and (2.3bar, 5.22K).

view, comparing it with a type of Bose-Einstein condensation (BEC) [1]. London’s theory has now been validated by many experiments. Meanwhile, the “two-fluid model” proposed by L. Tisza[2] and L. Landau [3], which assumes the coexistence of superfluidity and normal fluidity in liquid ^4He , has become the most acknowledged phenomenological description. In this model, the total mass density ρ is expressed as follows:

$$\rho = \rho_n + \rho_s, \quad (1)$$

where ρ_n and ρ_s are the mass densities of the normal fluid and of the superfluid, which respectively satisfy the

* The University of Tokyo:tsuzuki@jamology.rcast.u-tokyo.ac.jp

laws of mass and entropy conservations as follows:

$$\frac{\partial \rho}{\partial t} + \nabla \cdot (\rho_n \mathbf{v}_n + \rho_s \mathbf{v}_s) = 0, \quad (2)$$

$$\frac{\partial}{\partial t}(\rho\sigma) + \nabla \cdot (\rho\sigma\mathbf{v}_n) = 0. \quad (3)$$

Here, \mathbf{v}_n and \mathbf{v}_s are the velocities of the normal fluid and of the superfluid, respectively, while σ is the entropy density.

A remarkable achievement of the two-fluid model is that it connects the macroscopic perspective of thermodynamics with quantum mechanics, so that the superfluid can be described within a framework of basic mechanics. By solving the Gross-Pitaevskii equation (a nonlinear Schrödinger equation for boson particles) and the Gibbs-Duhem equation simultaneously, we obtain the following equations of motion for liquid ^4He from a phenomenological perspective [4]:

$$\rho_s \frac{D\mathbf{v}_s}{Dt} = -\frac{\rho_s}{\rho} \nabla P + \rho_s \sigma \nabla T, \quad (4)$$

$$\rho_n \frac{D\mathbf{v}_n}{Dt} = -\frac{\rho_n}{\rho} \nabla P - \rho_s \sigma \nabla T + \eta_n \nabla^2 \mathbf{v}_n, \quad (5)$$

where $D\{\cdot\}/Dt$ represents a material derivative, and \mathbf{v}_n and \mathbf{v}_s are the velocities of the normal fluid and superfluid, respectively. η_n is the viscosity of the normal fluid. T is temperature, P is pressure, and σ is entropy density.

Hydrodynamic aspects of liquid ^4He have been intensively studied through experiments involving counterflow in a cylinder attached to a reservoir of the liquid at one point and a heater at another point. Under this condition, the liquid ^4He is in a separate phase of super and normal fluids, which flow in the opposite direction [5]. C. J. Gorter and J. H. Mellink found the mutual friction forces to be the reason for the discrepancy in Eq. (4) and Eq. (5) with respect to the counterflow experiments at high heat fluxes [6], which are given as

$$\rho_s \frac{D\mathbf{v}_s}{Dt} = -\frac{\rho_s}{\rho} \nabla P + \rho_s \sigma \nabla T - \mathbf{F}_{sn}, \quad (6)$$

$$\rho_n \frac{D\mathbf{v}_n}{Dt} = -\frac{\rho_n}{\rho} \nabla P - \rho_s \sigma \nabla T + \eta_n \nabla^2 \mathbf{v}_n + \mathbf{F}_{sn}. \quad (7)$$

Further studies by W.F. Vinen [7] through experiments with the second sound wave attenuations revealed a detailed quantitative expression for \mathbf{F}_{sn} as

$$\mathbf{F}_{sn} = \frac{2}{3} \rho_s \alpha \kappa L \mathbf{v}_{sn}, \quad (8)$$

where ρ_s is the mass density of a superfluid, κ is the quantum of circulation, \mathbf{v}_{sn} is the relative velocity of $\mathbf{v}_s - \mathbf{v}_n$, α is a friction coefficient, and L is the vortex line density. It is known that L at the steady state can be described as

$$L^{-1}(t) = L^{-1}(0) + \beta_v t, \quad (9)$$

where β_v is a coefficient in the Vinen equation [8].

From the viewpoint of numerical research, finite approximation of the equations of motion in Eq. (6) and

Eq. (7) represents an essential step toward direct numerical simulations. However, to date, only a few studies have adopted such an approach; this is primarily because most previous works take a non-phenomenological point of view (e.g., numerical simulations of nonlinear Schrödinger equations [9, 10], and quantum Monte Carlo calculations [11, 12] aiming to examine the static responses [13] or to explore quantum vortices and turbulence [14–18]). Although previous works [19–23] introduce direct numerical simulations of the two-fluid model, they focus on mesh-based discretization; when simulating liquid ^4He , some studies [19–21] developed finite difference approximations, and others [22, 23] devised novel finite element approximations. Unfortunately, none of the previous studies have reported a finite particle approximation of these governing equations.

There are many advantages to numerical simulations using the finite particle approximation because of the discretization based on many-particle interacting systems. Each particle moves in space interacting with every other particle, taking either the state of a superfluid or normal fluid. The mechanical picture, in this case, is much closer to the view of quantum statistical systems that follow Bose-Einstein condensates, compared to the case of grid-based methods. Using the same number of particles as real atoms in liquid ^4He in simulations remains challenging even today. Nevertheless, finite particle approximation clearly has a high possibility of bridging the gulf between the phenomenological and microscopic concepts of liquid ^4He . Furthermore, from a practical aspect, the particle approximation is capable of handling complex boundaries. It has great potential to perform simulations realistic enough to reproduce an experimental setup. However, in addition to these potential advantages, the computational costs are much higher than with other methods. In addition, because the non-uniformity of particle distributions often causes deterioration of numerical accuracy, it is necessary to select appropriate supportive techniques to stabilize the simulations.

The main purpose of this study is to present a scheme for finite particle approximation of the two-fluid model. We propose to discretize the two-fluid model of superfluid ^4He using smoothed particle hydrodynamics (SPH) [24], a well-established Lagrangian particle approximation particularly popular in the field of astrophysics. By combining theoretical methodologies typical of two different branches of physics (low-temperature physics and astrophysics), we aim to pioneer a new paradigm of Lagrangian particle mechanics targeting superfluids.

The remainder of this article is structured as follows. Section II describes the concept of SPH, provides a summary of wave equations in superfluid ^4He , and discusses the expression of thermodynamic parameters in the two-fluid model, in preparation for Section III. In Section III, we derive a finite particle approximation of liquid ^4He . In Section IV, we discuss strategies for practical applications and introduce several improved numerical schemes for SPH. In Section V, we demonstrate our model with

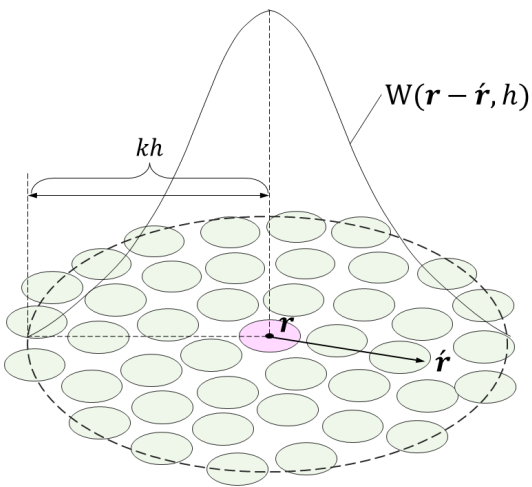


FIG. 2. Schematic of a kernel function.

two major numerical tests: the Rayleigh-Taylor instability and wave propagation analyses. Section VI summarizes our results and concludes the paper.

II. PREPARATIONS

II.1. A brief overview of SPH

The fundamental concept of SPH is the approximation of the Dirac delta function δ in integral form by a distribution function W , which is called the smoothed kernel function, as follows [24]:

$$\begin{aligned}\phi(\mathbf{r}) &= \int_{\Omega} \phi(\hat{\mathbf{r}}) \delta(\mathbf{r} - \hat{\mathbf{r}}) d\hat{\mathbf{r}} \\ &\simeq \int_{\Omega} \phi(\hat{\mathbf{r}}) W(\mathbf{r} - \hat{\mathbf{r}}, h) d\hat{\mathbf{r}},\end{aligned}\quad (10)$$

where ϕ is a physical value at the position \mathbf{r} in a domain Ω and the parameter h is called a kernel radius. The smoothed kernel function W must have at least the following four characteristics; (a) W converges to the delta function δ as h approaches 0 ($\lim_{h \rightarrow 0} W = \delta$); (b) W satisfies the normalization condition ($\int W d\mathbf{r} = 1$); (c) W satisfies the symmetricity $W(-\mathbf{r}) = W(\mathbf{r})$; and (d) W is such that the value of W becomes 0 at a distance kh , which is called a compact support condition. Figure 2 represents a schematic view of a kernel function. An example of a smoothed kernel function W is the Gaussian, which is simply expressed as

$$W(\mathbf{r}) := \frac{C}{h^d} e^{-(\mathbf{r}-\hat{\mathbf{r}})^2/h^2}, \quad (11)$$

where d is the dimension ($d = 1, 2,$ or 3) and C is a normalization factor. The Gaussian kernel is frequently used in the field of astrophysics. In the field of incompressible SPH, in contrast, polynomial functions are often used [25, 26].

Equation (10) is further discretized on the basis of the summation approximation using the position \mathbf{r}_j , the infinitesimal volume ΔV_j , density ρ_j , and mass m_j of the j th particle as follows.

$$\begin{aligned}\phi(\mathbf{r}_i) &\approx \sum_j^{N_p} \phi(\mathbf{r}_j) W(|\mathbf{r}_i - \mathbf{r}_j|, h) \Delta V_j \\ &= \sum_j^{N_p} \frac{\phi(\mathbf{r}_j)}{\rho_j} m_j W(|\mathbf{r}_i - \mathbf{r}_j|, h),\end{aligned}\quad (12)$$

where $m_j = \rho_j \Delta V_j$ and N_p is the number of fluid particles used to approximate the system. The gradient and the Laplacian of the physical value $\phi(\mathbf{r}_i)$ are axiomatically obtained from Eq. (12) using a vector analysis, as follows:

$$\nabla \phi(\mathbf{r}_i) = \rho_i \sum_j^{N_p} m_j \left(\frac{\phi(\mathbf{r}_i)}{\rho_i^2} + \frac{\phi(\mathbf{r}_j)}{\rho_j^2} \right) \nabla W_{ij}, \quad (13)$$

$$\nabla^2 \phi(\mathbf{r}_i) = \sum_j^{N_p} \frac{m_j}{\rho_j} \frac{\phi(\mathbf{r}_i) - \phi(\mathbf{r}_j)}{|\mathbf{r}_i - \mathbf{r}_j|^2} (\mathbf{r}_i - \mathbf{r}_j) \cdot \nabla W_{ij}, \quad (14)$$

where $W_{ij} = W(|\mathbf{r}_i - \mathbf{r}_j|, h)$. Here, we have used the mathematical relationship $\nabla f = \rho[\nabla(f/\rho) + (f/\rho^2)\nabla\rho]$ to derive Eq. (13), so that the gradient operator has symmetricity of pressures between the i th and j th particles. For more details of the operators in SPH, refer to [27].

II.2. Wave equations of superfluids

According to the literature [3], the governing equations of Eq. (2) to Eq. (5) yield wave propagation equations regarding density ρ and entropy S , which produce multiple types of sound waves. Under a first approximation that neglects the viscosity term, the wave equations give two different sound waves, expressed as follows [28, 29]:

$$c_1 = \left(\frac{\partial P}{\partial \rho} \right)_S^{1/2}, \quad (15)$$

$$c_2 = \left(\frac{\rho_s T S^2}{\rho_n C_v} \right)^{1/2}, \quad (16)$$

where c_1 and c_2 are called the first sound velocity and the second sound velocity, respectively. C_v represents the specific heat at constant volume. Equation (16) can be rewritten using the number of ^4He atoms N and the mass of a ^4He atom M as

$$\frac{\rho_s}{\rho_n} = \left\{ \frac{C_v c_2^2}{(NM)^2 T \sigma^2} \right\}, \quad (17)$$

where we have introduced a basic relation between the entropy density σ and the entropy S of $\sigma = S/(NM)$.

II.3. Expression of thermodynamic variables in an elementary excitation model

As a consequence of the two-fluid model by L. Landau, it was found that the elementary excitation of liquid ^4He is derived from two components, “phonons” and “rotons” [3]. The pressure P of liquid ^4He can thus be expressed as follows [30]:

$$P = P_{\text{ph}} + P_{\text{rot}}. \quad (18)$$

Here, let us denote the ratio of a circle’s circumference as π , and the speed of sound as c . We also introduce constant values for μ , p_0 , and Δ as 1.72×10^{-24} g, 2.1×10^{-19} g cm^{-1} , and 8.9 K, respectively, according to the literature [31, 32]. When $T \ll 93$ K, Eq. (18) can be approximated as [30, 31]:

$$P \simeq \frac{\pi^2 (k_B T)^4}{90 \hbar^3 c^3} + \frac{p_0^2 \sqrt{(\pi \mu / 2)}}{2\pi^2 \hbar^3} (k_B T)^{3/2} e^{-\Delta/T}, \quad (19)$$

where k_B represents the Boltzmann constant and \hbar is the reduced Planck’s constant. Note that Eq. (19) is similar to Eq. (5) in the literature [30]. The entropy S is obtained from the first-order partial derivatives of P with respect to temperature T as

$$S := \left(\frac{\partial P}{\partial T} \right) \quad (20)$$

$$\simeq \frac{2\pi^2 k_B^4 T^3}{45 \hbar^3 c^3} + \left(\frac{k_B}{2\pi} \right)^{3/2} \frac{\sqrt{\mu p_0^2 \Delta} e^{-\Delta/T}}{\hbar^3 \sqrt{T}}, \quad (21)$$

where we have ignored higher-order terms in the derivation of the second term in Eq. (21).

Accordingly, the entropy density σ is obtained using the relation $\sigma = S/(NM)$ as

$$\sigma = \zeta T^3 + \xi \frac{e^{-\Delta/T}}{T^{1/2}}, \quad (22)$$

$$\zeta := \frac{2\pi^2 k_B^4}{45 \hbar^3 c^3 NM}, \quad (23)$$

$$\xi := \left(\frac{k_B}{2\pi} \right)^{3/2} \frac{\sqrt{\mu p_0^2 \Delta}}{\hbar^3 NM}. \quad (24)$$

Here, both ζ and ξ are constant parameters because their components of N , M , π , c , μ , p_0 , Δ , k_B , and \hbar are all constant and can be given as known parameters. Now, we have prepared all the parameters needed for the derivation of a particle approximation of liquid ^4He .

III. DISCRETIZATION OF THE TWO-FLUID MODEL USING STANDARD SPH

First, Eq. (6), the motion equation for superfluid components, can be rewritten as:

$$\frac{D\mathbf{v}_s}{Dt} = -\frac{1}{\rho} \nabla P + \sigma \nabla T - \frac{1}{\rho_s} \mathbf{F}_{sn}. \quad (25)$$

Using Eq. (13), we obtain the particle discretization of the right-hand side of Eq. (25), with respect to the i th particle, as follows:

$$\left\langle -\frac{1}{\rho} \nabla P \right\rangle_i = -\sum_j m_j \left(\frac{P_i}{\rho_i^2} + \frac{P_j}{\rho_j^2} \right) \nabla W_{ij}, \quad (26)$$

$$\left\langle \sigma \nabla T \right\rangle_i = \theta_i^s \sum_j m_j \left(\frac{T_i}{\rho_i^2} + \frac{T_j}{\rho_j^2} \right) \nabla W_{ij}, \quad (27)$$

where θ_i^s is represented using Eq. (22) as

$$\theta_i^s = \rho_i \sigma_i. \quad (28)$$

Here, the superscript of θ_i^x represents the first letter of “superfluid” or “normal fluid” ($x = s, n$). The detailed evaluation of σ_i is discussed in Section IV.2.

The two-way coupling technique for SPH [33, 34] in basic mechanics to compute relative velocity between two phases can be applied to the discretization of \mathbf{F}_{sn} . From Eq. (8), a mutual friction force $\mathbf{F}_s^{(i)}$ of the i th superfluid particle is obtained as follows:

$$\mathbf{F}_s^{(i)} = C_L \frac{\sum_{j \in \Omega_i} (\mathbf{v}_s^{(i)} - \mathbf{v}_n^{(j)}) W_{ij}}{\sum_{j \in \Omega_i} W_{ij}}, \quad (29)$$

where C_L is $2/3 \rho_s \alpha \kappa L$ and Ω_i is the set of all the particles in the neighborhood of the i th normal fluid particles. The third term on the right-hand side in Eq. (25) is obtained by dividing Eq. (29) by $-\rho_s^{-1}$.

Second, Eq. (7), the motion equation for normal fluid components, can be rewritten as:

$$\frac{D\mathbf{v}_n}{Dt} = -\frac{1}{\rho} \nabla P - \frac{\rho_s}{\rho_n} \sigma \nabla T + \frac{\eta_n}{\rho_n} \nabla^2 \mathbf{v}_n + \frac{1}{\rho_n} \mathbf{F}_{sn}. \quad (30)$$

The first term on the right-hand side in Eq. (30) can be discretized similar to the case of Eq. (26). Meanwhile, the discretized expression of the second term with respect to the i th particle is obtained using Eq. (13) as follows.

$$\left\langle -\frac{\rho_s}{\rho_n} \sigma \nabla T \right\rangle_i = \theta_i^n \sum_j m_j \left(\frac{T_i}{\rho_i^2} + \frac{T_j}{\rho_j^2} \right) \nabla W_{ij}, \quad (31)$$

where the breakdown of θ_i^n is given as

$$\theta_i^n = \chi \frac{\rho_i}{T_i \sigma_i}, \quad (32)$$

$$\chi := \frac{C_v c_2^2}{(NM)^2}. \quad (33)$$

Meanwhile, a substitution of Eq. (14) into the third term directly leads to:

$$\left\langle \frac{\eta_n}{\rho_n} \nabla^2 \mathbf{v}_n \right\rangle_i = 2\nu_n \sum_j \frac{m_j}{\rho_j} \frac{\mathbf{v}_n^{(i)} - \mathbf{v}_n^{(j)}}{|\mathbf{r}_i - \mathbf{r}_j|^2} (\mathbf{r}_i - \mathbf{r}_j) \cdot \nabla W_{ij}, \quad (34)$$

where ν_n is the kinetic viscosity, which is equal to η_n/ρ_n . Subsequently, the mutual friction force $\mathbf{F}_n^{(j)}$ of the j th

normal fluid particle is obtained by summing up the contributions from each reaction force of the i th superfluid particle as follows:

$$\mathbf{F}_n^{(j)} = - \sum_{i \in \Omega_j} \mathbf{F}_s^{(i)} \left(\frac{W_{ij}}{\sum_{k \in \Omega_i} W_{ik}} \right), \quad (35)$$

where Ω_j is the set of all particles in the neighborhood of the j th normal fluid particle, while Ω_i is that of the i th superfluid particle. Note that the summation inside the brackets in Eq. (35) is with respect not to j but to i in order for the two phases to conserve an equal amount of momentum exchange. In the end, the fourth term on the right-hand side in Eq. (30) is obtained by dividing Eq. (35) by ρ_n^{-1} .

Now, the right-hand sides of Eq. (25) and Eq. (30) are appropriately discretized. The material derivative of velocities in the left-hand sides of Eq. (25) and Eq. (30) can be discretized using an explicit time-integrating scheme, e.g., the Verlet algorithm [35], in accordance with the usual manner in SPH simulations. Consequently, we have successfully derived a particle approximation of the governing equations of liquid ^4He .

IV. STRATEGIES FOR PRACTICAL APPLICATION

IV.1. Introduction of improved techniques to stabilize the simulations

It is known that the standard SPH only permits a slight density difference between two phases when being applied to multi-phase flow problems because it does not assume a larger density gradient than that of the gradient of the smoothing kernel function in its formulation [36]. As a remedial measure, we introduce an improved SPH scheme that ensures the continuity of the pressure and pressure gradient at the interface between two phases, while satisfying mass and momentum conservation [37]. In this method, the density of the i th particle is computed as follows:

$$\rho_i = m_i \sum_j W(|\mathbf{r}_i - \mathbf{r}_j|, h). \quad (36)$$

Instead of Eq. (26), the pressure gradient term is then computed as

$$\left\langle -\frac{1}{\rho} \nabla P \right\rangle_i = -\frac{1}{m_i} \sum_j \left(\frac{m_i^2}{\rho_i^2} + \frac{m_j^2}{\rho_j^2} \right) \tilde{P} \nabla W_{ij}, \quad (37)$$

where \tilde{P} is the reduced pressure, given as

$$\tilde{P} := \frac{\rho_i P_j + \rho_j P_i}{\rho_i + \rho_j}. \quad (38)$$

Similarly, the following equation is used to compute the viscosity term instead of Eq. (34):

$$\left\langle \frac{\eta_n}{\rho_n} \nabla^2 \mathbf{v}_n \right\rangle_i = \frac{\eta_n}{m_i} \sum_j \left(\frac{m_i^2}{\rho_i^2} + \frac{m_j^2}{\rho_j^2} \right) \frac{\mathbf{v}_n^{(ij)}}{|\mathbf{r}_{ij}|^2} \mathbf{r}_{ij} \cdot \nabla W_{ij}, \quad (39)$$

where $\mathbf{v}_n^{(ij)}$ and \mathbf{r}_{ij} are respectively given as

$$\begin{aligned} \mathbf{v}_n^{(ij)} &:= \mathbf{v}_n^{(i)} - \mathbf{v}_n^{(j)}, \\ \mathbf{r}_{ij} &:= \mathbf{r}_i - \mathbf{r}_j. \end{aligned} \quad (40)$$

Additionally, several sophisticated techniques are appropriately introduced. First, we use a pair-wise particle collision technique [38] that gives a repulsive force when two particles are too close to each other. Specifically, the momentum conservation in the normal direction between two colliding particles is computed using this technique. Next, we introduce a one-dimensional Riemann solver [39] in each pair-wise particle, instead of using artificial viscosities. These two supportive techniques become valid only when the two particles are closer to each other than a distance equal to the initial particle distance d , as exceptional cases.

Meanwhile, we set the time increment δt to be as small as about one-twentieth of the three conditions of numerical stability, the CFL (Courant-Friedrichs-Lewy) condition, diffusion condition, and body force condition [40], because it is possible for SPH simulations using the explicit time-integrating scheme to violate energy conservation. Regarding entropy conservation, we set constant values for the particles in the initial state and keep the values during simulations; this is further explained in the next section.

IV.2. Entropy density estimation

It can be said from Eq. (27) and Eq. (31) that each of θ_i^s and θ_i^n functions as a parameter that determines the degree of the effect of temperature gradient forces. The entropy density σ_i is dominant in the behavior of θ_i^s because the density ρ_i fluctuates typically less than one percent compared with its averaged density in incompressible SPH [41, 42]. Additionally, the behavior of σ corresponds to that of entropy S because the value of NM is constant; thus, θ_i^s is proportional to the entropy S . Figure 3(a) shows the dependence of entropy S on temperature T , indicating that the effect of the temperature gradient force controlled by θ_i^s on the superfluid component diminishes as the temperature T decreases, and it eventually reaches zero at absolute zero. Based on the result, we can say that the parameter θ_i^s reflects well the characteristic that superfluids have almost zero or a very small temperature gradient, corresponding to extremely high heat conductivity.

Regarding the parameter θ_i^n , the second sound velocity c_2 of Eq. (33) should be semi-empirically determined according to the literature, exemplified by [43, 44]. In experiments, it is known that c_2 emerges when the system reaches temperatures lower than the critical temperature of approximately 2.17 K, increases as the cooling of the system increases, and finally reaches approximately 135 ms^{-1} after experiencing a sluggishness at approximately 20 ms^{-1} [44]. Let us assume in this discussion that c_2 is constant. In this ideal case, the parameter χ becomes constant; thus, θ_i^n becomes proportional to

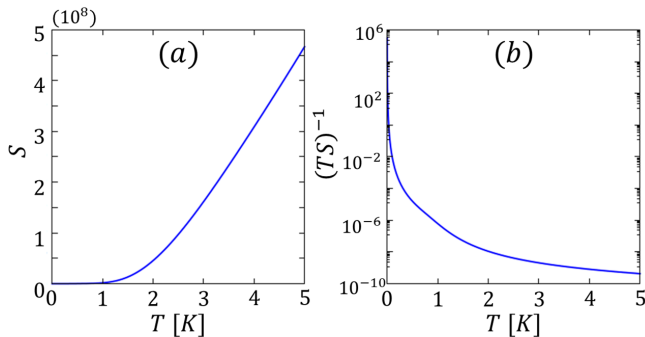


FIG. 3. Dependences of (a) the entropy S and (b) $(TS)^{-1}$ on the temperature T .

$(T_i \sigma_i)^{-1}$. Also, the behavior of σ corresponds to that of entropy S , similar to the case of θ_i^s . After all, the behavior of θ_i^n is determined by that of $(TS)^{-1}$. Figure 3(b) shows the dependence of $(TS)^{-1}$ on the temperature T with a semi-logarithmic scale. The effect of θ_i^n on fluid ${}^4\text{He}$ is confirmed to greatly increase as the temperature T_i decreases. Remember that the parameter θ_i^n is the discretized formula of Eq. (17), expressing the ratio of superfluid density to normal density, which generates the second sound wave. Figure 3(b) suggests that the effect of ρ_s/ρ_n increases as the temperature T decreases, on the premise that c_2 is constant; the effect is more amplified in actual cases because the velocity c_2 itself increases, as mentioned above [44].

As discussed above, both parameters θ_i^s and θ_i^n are confirmed to reflect the phenomenological behavior of superfluid ${}^4\text{He}$ qualitatively. However, it is also found that θ_i^n is too sensitive to be used for practical applications. As a remedy, we give the parameters of ρ_s and ρ_n as constant initial parameters; we compute Eq. (31) from Eq. (27) multiplied by $-\rho_s/\rho_n$. We also compute the entropy σ_i in the parameter θ_i^s from Eq. (22) scaled by a coefficient of C_e as

$$\sigma_i = C_e \sigma. \quad (41)$$

Here, the reason we introduce C_e is because Eq. (21) does not consider the effect of interactions among particles in its derivation. In that sense, Eq. (21) can be said to express a relationship between entropy and temperature in a quantum ideal gas. Hence, it is necessary to consider the volume ratio of gas to a liquid. In this article, we estimate the value of C_e as the volume ratio of gas to liquid, each of which has the same density under a certain pressure ($C_e \approx V_{\text{liquid}}/V_{\text{air}}$), as the first approximation level.

IV.3. The variables of the system

The variables for the i th particle are given as a set of $(\mathbf{r}_i, \mathbf{v}_n^{(i)}, \mathbf{v}_s^{(i)}, m_i, \rho_i, \sigma_i, P_i, T_i)$. P_i is calculated from ρ_i by solving a one-to-one thermodynamic correspondence between P_i and ρ_i given by the Tait equation of state [45].

Meanwhile, ρ_i and σ_i are calculated using Eq. (36) and Eq. (41), respectively. m_i and T_i keep their initial values in this paper. $\mathbf{v}_s^{(i)}$ and $\mathbf{v}_n^{(i)}$ are not necessarily distinguished in implementations because each particle only takes either a superfluid or normal fluid state at a time. Thus, the variable of the i th particle can be reduced to the set of $(\mathbf{r}_i, \mathbf{v}_i, m_i, \rho_i, \sigma_i, P_i, T_i)$.

The parameter C_L includes one time-dependent parameter of the vortex line density L and three other constant values: the superfluid density ρ_s , a friction coefficient α , and the quantum of circulation κ , where L is calculated from Eq. (9) at every time step. In this article, the parameter β_v of Eq. (9) is calculated according to Table 1 and Table 3 in the literature [46]. To summarize, the constant parameters characterizing the system are given as a set of $(N, M, \rho_s, \rho_n, T_0, C_e, \nu_n, c, \alpha, \beta_v, \kappa, L_0)$, where $L_0 = L(0)$ of Eq. (9). The exact constant values that are independent of the system are $(\mu, p_0, \Delta, k_B, \hbar)$.

V. NUMERICAL ANALYSES

In this section, we demonstrate our method by performing two major numerical tests: the Rayleigh-Taylor instability (RTI) and entropy wave propagation analyses. The linear growth of the mushroom structure similar to that in classical fluids has been reported to be observed in the direct simulation of the Gross-Pitaevskii equation [47]. In Section V.1, we examine whether we can find the emergence of the linear growth of the mushroom structure on the condition of a completely separate state of superfluid and normal fluid (NS counterflow), using the proposed model. Meanwhile, simulating wave propagation is challenging for the SPH, particularly in the case of an explicit time-integrating scheme. We discuss the applicability of SPH to entropy wave propagation problems by examining the effect of density fluctuations on the error in calculations with a hypothetical case in Section V.2.

V.1. Rayleigh-Taylor instability simulation

We set the simulation domain of (L_x, L_y) to be $(1.0, 2.0)$ and place the superfluid particles at $y > 0.5L_y$ and the normal fluid particles at $y < 0.5L_y$. We set the resolution of (N_{px}, N_{py}) to be $(240, 480)$, where N_{px} and N_{py} are the number of particles arranged in each direction. The interface between the two phases is disturbed by the function $y = L_x(1.0 - 0.15\sin(2.0\pi x/L_x))$, and the value of the gravity constant of 0.09 m/s^2 is set in the y -direction, in a manner similar to the case in a classical fluid [48]. We arrange multiple layers of frozen particles as walls, alongside the boundary of the simulation domain. No-slip conditions are imposed on the wall particles as boundary conditions. The reference temperature T_0 is set to be 1.6 K . Using T_0 , we set the temperature of superfluid particles to be $T_0 \times 0.99$ and set that of normal fluid particles to be $T_0 \times 1.01$. The parameters

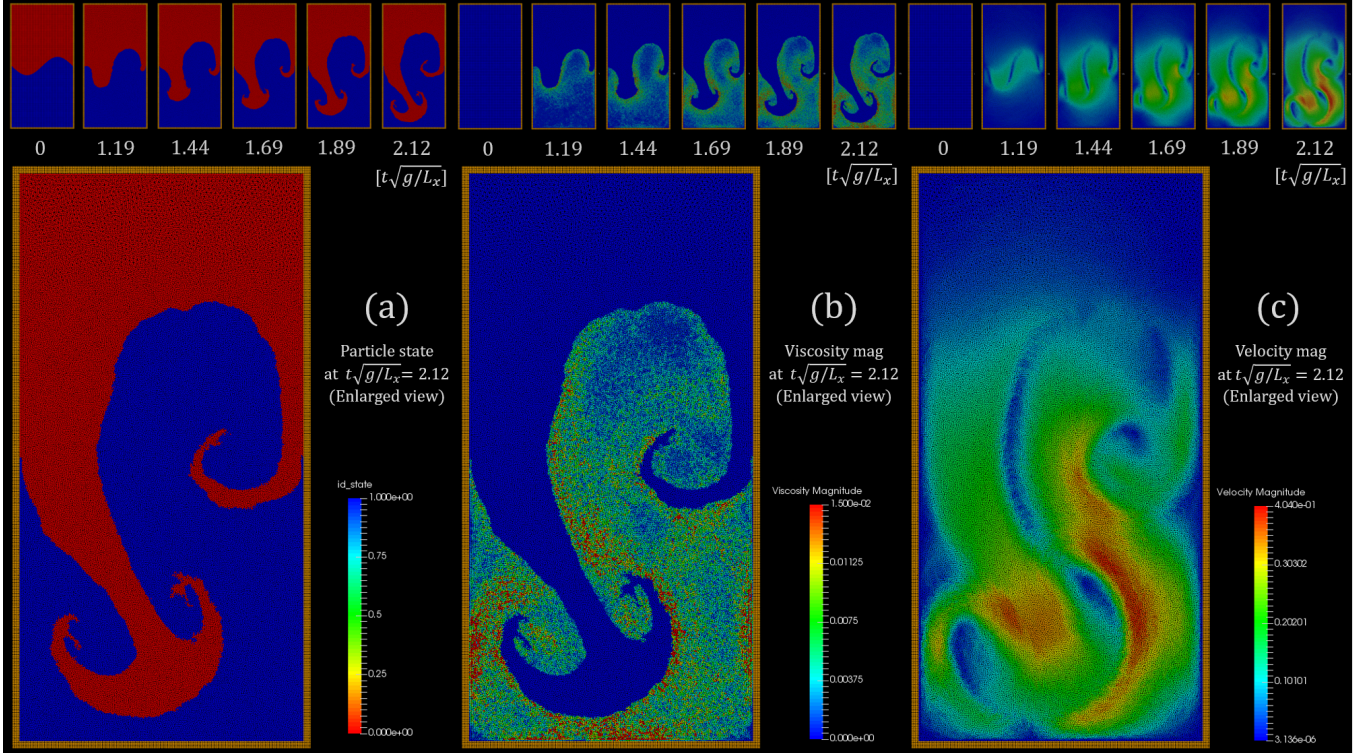


FIG. 4. Snapshots of the Rayleigh-Taylor instability simulation until the emergence of linear growth of the mushroom structure when setting (N_{px}, N_{py}) to be $(240, 480)$ and setting the density ratio to be $\rho_s/\rho_n = 5.024$.

$(\rho_s, \rho_n, \alpha, \beta_v, \kappa, \mu_n)$ are determined by reference to the values in Table 1 and Table 2 in the literature [46] in the case of $T_0 = 1.6$ K. The resulting density ratio of ρ_s/ρ_n becomes 5.024. Meanwhile, we set the vortex line density L_0 to be $1 \times 10^6 \text{ cm}^{-1}$ as an initial state, in reference to the literature [8]. We estimate the dimensionless parameter C_e to be 1.428×10^{-3} considering the volume ratio of $V_{\text{liquid}}/V_{\text{air}}$ at 1.01325 bar [49]. The value of NM in Eq. (22) is set equivalent to $\rho_n L_x^2$ because only the normal fluid components carry entropy.

Figure 4 shows snapshots of the Rayleigh-Taylor instability simulation. The red part and blue part in Fig. 4(a) respectively represent the superfluid particles and normal particles. As a result, we confirmed the emergence of the characteristic mushroom structure in the linear growth regime. The mushroom structure shows its growth in the slanting direction because of wall boundary conditions; this is the same as the case for a classical fluid [50]. The time from the start to the final snapshot is approximately 7.07 s in physical time, which corresponds to approximately 2.12 in the time scaled by the factor $\sqrt{(g/L_x)}$. Figure 4(b) represents the magnitude of the viscosity term calculated using Eq. (39); the magnitude of viscosity is confirmed to be zero in normal fluid components. Fig. 4(c) shows the magnitude of the velocity of particles for reference.

To discuss the state after further time evolution, it is necessary to introduce the state transition between superfluid and normal fluid particles. In this case, each particle stochastically changes its state according to quantum statistical mechanics; the most straightforward approach is to estimate the probability of transition using the distribution of Bose-Einstein condensates. Suitable transition models should be discussed in future studies.

V.2. Effect of density fluctuations on the numerical analysis of the entropy wave equation

Let us examine the effect of density fluctuations on the calculation error of wave propagation problems with a hypothetical case. The wave equation is given as

$$\frac{\partial^2 S}{\partial t^2} = c^2 \nabla^2 S, \quad (42)$$

where c is the speed of sound. We impose closed boundary conditions:

$$S(x, 0) = S(x, L_y) = 0, \quad (43)$$

$$S(0, y) = S(L_x, y) = 0. \quad (44)$$

In this case, the analytical solution of Eq. (42) is given as follows [51]:

$$S(x, y) = A(t) \sin \frac{m\pi x}{L_x} \sin \frac{n\pi y}{L_y} \begin{pmatrix} m = 1, 2, \dots \\ n = 1, 2, \dots \end{pmatrix}, \quad (45)$$

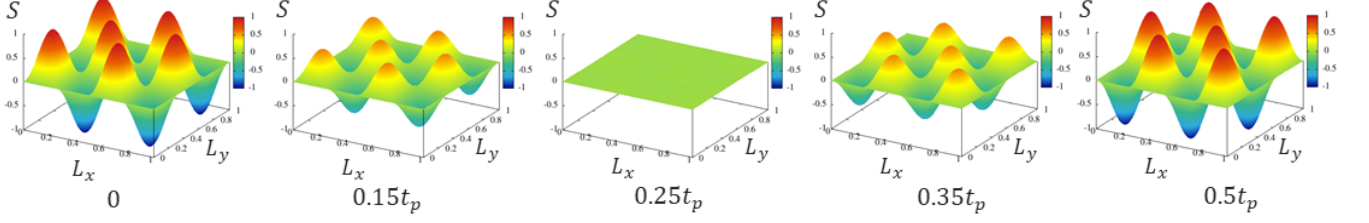


FIG. 5. Snapshots of the analytical solution of the targeted problem during the time from 0 s to the half-period of time.

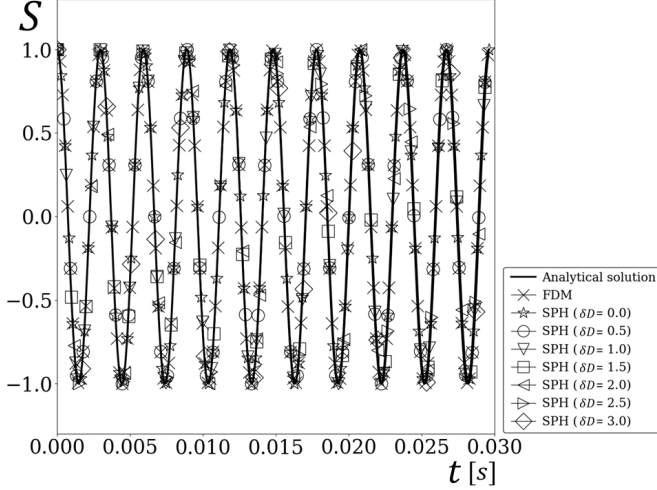


FIG. 6. Variation of S at a certain point during the simulation with $C_s = 135$ in the cases of FDM or SPH with different values of δD .

where the time-dependent function $A(t)$ is expressed as

$$A(t) = C_{m,n} \sin \lambda_{m,n} t + C_{m,n}^* \cos \lambda_{m,n} t, \quad (46)$$

$$\lambda_{m,n} = c\pi \sqrt{\frac{m^2}{L_x^2} + \frac{n^2}{L_y^2}}. \quad (47)$$

Here, $C_{m,n}$ and $C_{m,n}^*$ correspond to the coefficients of the sine terms and cosine terms in the double Fourier expansion of Eq. (45), respectively. In this benchmark test, we discretize the left-hand side of Eq. (42) using the second-order central difference method [52] while replacing the right-hand side with the Laplacian operators of SPH or the finite-difference method (FDM); we can focus on the problem of numerical error in the spatial direction.

We set the simulation domain of (L_x, L_y) to be $(1.0, 1.0)$ and set the resolution of (N_{px}, N_{py}) to be $(400, 400)$. We take two cases, setting the speed of sound c to be 135 ms^{-1} and 20 ms^{-1} , assuming two representative cases of the second sound waves of ^4He in the low-temperature region, as mentioned in Section IV.2. We set the pair of (m, n) to be $(4, 3)$ and set the initial velocity of each particle to be 0 everywhere in the simulation domain. In this case, the values of $C_{m,n}$ and $C_{m,n}^*$ become 0 and 1. Figure 5 shows snapshots of the analytical

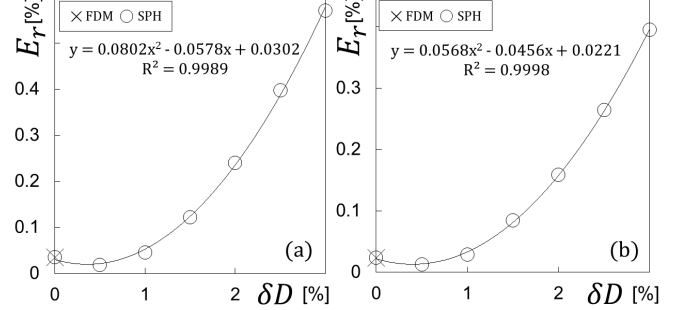


FIG. 7. Dependence of the relative error E_r on the parameter δD : (a) for $C_s = 135$ and (b) $C_s = 20$.

solution of the targeted problem during the time from 0 s to the half-period of time.

In SPH, we set the same mass for all the particles. In this case, only the non-uniformity of particle arrangements contributes to the fluid density fluctuation because of the weighted calculation according to the positions of particles. Let us introduce the initial distance between two particles, l , and a distance parameter dl . Consider the case where we isotropically arrange particles with an interval of l in each direction and shift the particles by dl in an arbitrary direction. In this case, the averaged small volume ΔV_0 is l^2 , and the maximum one ΔV is $(l + dl)^2$. We define a volume fluctuation rate δD as $((\Delta V) - \Delta V_0) / \Delta V_0 \times 100$. Because of the uniformity of mass and the relationship $\Delta V = m/\rho$, it is possible for us to regard δD as a criterion for density fluctuation. Additionally, the physical time is set to 0.03 s, roughly assuming the time from the emergence of the second wave to the decay of the vortex line density [8]. In addition, we introduce a stabilization technique presented in the MPS (moving particle semi-implicit) [53] to suppress the increase in variance caused by repeated calculations (see Appendix A). We then compare the simulation results of SPH with that of FDM and the analytical solutions given by Eq. (45).

Figure 6 shows the variation of S at a certain point during the simulation with $C_s = 135$, in the respective cases. The solid line indicates the analytical solution, and the solid line with the cross symbol shows the simulation result of FDM. The remaining seven lines with symbols

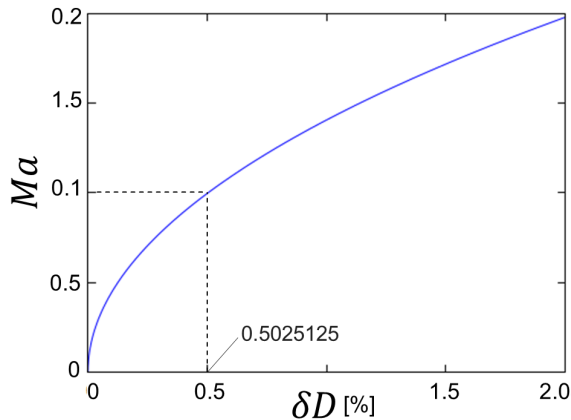


FIG. 8. Relationship between the mach number Ma and the parameter δD .

indicate the simulation results of SPH with different values of δD between 0 and 3 per cent. All results were confirmed to show excellent agreement at this viewing scale.

Fig. 7(a) shows further analyses of the results in Fig. 6, demonstrating the dependence of the relative error on the parameter δD in the respective cases. Here, the relative error E_r is defined as the average of $|S_i - S_a|/|S_a + A| \times 100$ over all the particles, where S_i is the value of S of the i th particle and S_a is the analytical value of the point on the particle. A is the amplitude of the oscillation, which is equivalent to 1 in this case and is added to the denominator to avoid division by zero. The solid curve indicates the fitting curves using the least squares method. The relative error δD in the case of SPH was found to be a minimum at approximately $\delta D = 0.5$; subsequently, it increased as δD increased by a power of two. Meanwhile, Fig. 7(b) shows the simulation results in the case where $C_s = 20$. The dependence of E_r on the parameter δD shows the same increase as in the case where $C_s = 135$.

The results in Fig. 7 demonstrate the applicability of SPH to wave propagation problems of liquid ^4He , even though the relative error E_r depends on the parameter δD by a power of two. This occurs because the relative error is small enough to be less than 0.25 per cent, even in the case where $\delta D = 2$. Here, δD is known to be approximately 0.5, in usual cases. Thus, the relative error is approximately 0.012 per cent for $C_s = 20$, and 0.018 per cent for $C_s = 135$. Through the discussion in this section, it is shown that we can perform wave propagation analyses within the range of these permissible errors.

The reason why δD is estimated to be 0.5 is explained as follows. The Mach number, the ratio of the maximum velocity to the speed of sound, is denoted as Ma . Given that the temperature is constant, the relative error of density is proportional to the square of Ma , which is described as $(\rho_0 - \rho)/\rho_0 = 0.5Ma^2$ as in [54]. Because of the uniformity of mass, we can obtain the relationship $2(1 - \Delta V_0/\Delta V) = Ma^2$, where $\Delta V_0 = m/\rho_0$ and $\Delta V = m/\rho$. Because ΔV_0 is l^2 and ΔV is $(l + dl)^2$,

a simple calculation leads to the following relationship between δD and Ma :

$$Ma = \sqrt{2\left(1.0 - \frac{1}{\delta D/100 + 1.0}\right)}. \quad (48)$$

Figure 8 shows the relationship between Ma and δD described by Eq. (48). In the simulation of incompressible SPH, Ma is given as an input parameter, which is typically set to 0.1. The value of δD at this time is approximately 0.5, as shown in Fig. 8.

VI. CONCLUSIONS

In this paper, we have theoretically derived a finite particle approximation of the two-fluid model of superfluid ^4He using smoothed particle hydrodynamics. To solve the governing equations, we introduced an auxiliary equation that represents a microscopic relationship between entropy and temperature derived from quantum statistical mechanics, in elementary particle physics. In numerical simulations, several sophisticated techniques have been appropriately introduced. In particular, we utilized a Riemann solver among neighboring particles to stabilize the simulation, as an alternative to artificial viscosity.

We have focused on the state of complete phase separation and demonstrated a Rayleigh-Taylor instability simulation. As a result, we confirmed the emergence of the characteristic mushroom structure in the linear growth regime. Furthermore, we discussed the applicability of SPH to entropy wave propagation analyses by examining the effect of density fluctuations on the error of calculations with a benchmark case. The simulation results show good agreement with those of FDM and with the analytical solution.

Consequently, our simulation model has been confirmed to reproduce the phenomenological characteristics of superfluid ^4He . We have thus pioneered a new paradigm of the Lagrangian particle mechanics, which will hopefully stimulate further numerical studies of superfluids in condensed matter physics.

ACKNOWLEDGEMENT

This research was supported by JSPS KAKENHI Grant Number 19K21528, and partly supported by ‘‘Grant-in-Aid for JSPS Fellows’’ in Japan. The author would like to thank Editage (www.editage.jp) for English language editing. The author would also like to express his gratitude to his family for their moral support and warm encouragement.

Appendix A: A reformulation of the Laplacian operator on the basis of MPS formalism

Equation (14) is reposted as

$$\nabla^2 \phi(\mathbf{r}_i) = \sum_j^{N_p} \frac{m_j}{\rho_j} \frac{\phi(\mathbf{r}_i) - \phi(\mathbf{r}_j)}{|\mathbf{r}_{ij}|^2} \mathbf{r}_{ij} \cdot \nabla W_{ij}, \quad (\text{A1})$$

where $\mathbf{r}_{ij} = \mathbf{r}_i - \mathbf{r}_j$. In the case where all particles have the same mass and density, we can replace m_j/ρ_j by m_i/ρ_i in Eq. (A1) as follows:

$$\nabla^2 \phi(\mathbf{r}_i) = \sum_j^{N_p} \frac{m_i}{\rho_i} \frac{\phi(\mathbf{r}_i) - \phi(\mathbf{r}_j)}{|\mathbf{r}_{ij}|^2} \mathbf{r}_{ij} \cdot \nabla W_{ij}, \quad (\text{A2})$$

Consider the functions:

$$\mathbb{P}_{ij} := \frac{w(\mathbf{r}_{ij})}{\sum_j w(\mathbf{r}_{ij})}, \quad (\text{A3})$$

$$w(\mathbf{r}_{ij}) := -\frac{1}{2D_s} \mathbf{r}_{ij} \cdot \nabla W_{ij}, \quad (\text{A4})$$

where D_s is the dimension. Equation (A3) can be regarded as a probability function when $w(\mathbf{r}_{ij})$ is positive everywhere in the neighborhood of the i th particle. To give examples, the Gaussian kernel and B-spline kernel

satisfy this condition. Because of the uniformity of mass, we can select a set of the density and small volume of the i th particle that has the relationship as

$$\rho_i = \frac{m_i}{\Delta V_i}, \quad (\text{A5})$$

$$\Delta V_i = \frac{1}{\sum_j w(\mathbf{r}_{ij})}. \quad (\text{A6})$$

From Eq. (A3) to Eq. (A6), Eq. (A2) is rewritten as

$$\nabla^2 \phi(\mathbf{r}_i) = 2D_s \sum_j^{N_p} \frac{\phi(\mathbf{r}_j) - \phi(\mathbf{r}_i)}{|\mathbf{r}_{ij}|^2} \mathbb{P}_{ij}. \quad (\text{A7})$$

Here, we replace the variance $|\mathbf{r}_{ij}|^2$ by its averaged expectation as

$$\nabla^2 \phi(\mathbf{r}_i) = \frac{2D_s}{\tau} \sum_j^{N_p} (\phi(\mathbf{r}_j) - \phi(\mathbf{r}_i)) \mathbb{P}_{ij}, \quad (\text{A8})$$

$$\tau = \sum_j |\mathbf{r}_{ij}|^2 \mathbb{P}_{ij}. \quad (\text{A9})$$

Note that the final forms of Eq. (A8) and Eq. (A9) are irrelevant to the choices of ρ_i and ΔV_i . The introduction of τ is known to suppress the increase in variance caused by repeated calculations [53, 55].

-
- [1] Bose, Plancks gesetz und lichtquantenhypothese, Zeitschrift für Physik **26**, 178 (1924).
- [2] L. TISZA, Transport phenomena in helium ii, Nature **141**, 913 (1938).
- [3] L. Landau, Theory of the superfluidity of helium ii, Phys. Rev. **60**, 356 (1941).
- [4] M. Tsubota, K. Fujimoto, and S. Yui, Numerical studies of quantum turbulence, Journal of Low Temperature Physics **188**, 119 (2017).
- [5] J. Tough, Chapter 3: Superfluid turbulence, volume 8 of *Progress in Low Temperature Physics*, pp. 133 – 219, Elsevier, 1982.
- [6] C. Gorter and J. Mellink, On the irreversible processes in liquid helium ii, Physica **15**, 285 (1949).
- [7] W. F. Vinen and D. Shoenberg, Mutual friction in a heat current in liquid helium ii i. experiments on steady heat currents, Proceedings of the Royal Society of London. Series A. Mathematical and Physical Sciences **240**, 114 (1957).
- [8] S. K. Nemirovskii, Quantum turbulence: Theoretical and numerical problems, Physics Reports **524**, 85 (2013), Quantum Turbulence: Theoretical and Numerical Problems.
- [9] L. Lehtovaara, T. Kiljunen, and J. Eloranta, Efficient numerical method for simulating static and dynamic properties of superfluid helium, Journal of Computational Physics **194**, 78 (2004).
- [10] I. Danaila and F. Hecht, A finite element method with mesh adaptivity for computing vortex states in fast-rotating bose-einstein condensates, Journal of Computational Physics **229**, 6946 (2010).
- [11] D. CEPERLEY and B. ALDER, Quantum monte carlo, Science **231**, 555 (1986).
- [12] J. Casulleras and J. Boronat, Unbiased estimators in quantum monte carlo methods: Application to liquid ^4He , Phys. Rev. B **52**, 3654 (1995).
- [13] S. Moroni, D. M. Ceperley, and G. Senatore, Static response from quantum monte carlo calculations, Phys. Rev. Lett. **69**, 1837 (1992).
- [14] S. A. Vitiello, L. Reatto, G. V. Chester, and M. H. Kalos, Vortex line in superfluid ^4He : A variational monte carlo calculation, Phys. Rev. B **54**, 1205 (1996).
- [15] S. K. Nemirovskii and W. Fiszdon, Chaotic quantized vortices and hydrodynamic processes in superfluid helium, Rev. Mod. Phys. **67**, 37 (1995).
- [16] R. J. Donnelly, *Quantized vortices in helium II* volume 2 (Cambridge University Press, 1991).
- [17] L. Vranješ, J. Boronat, J. Casulleras, and C. Cazorla, Quantum monte carlo simulation of overpressurized liquid ^4He , Phys. Rev. Lett. **95**, 145302 (2005).
- [18] D. E. Galli, L. Reatto, and M. Rossi, Quantum monte carlo study of a vortex in superfluid ^4He and search for a vortex state in the solid, Phys. Rev. B **89**, 224516 (2014).
- [19] Y. S. Ng, J. H. Lee, and W. F. Brooks, Numerical modeling of helium-ii in forced flow conditions, Journal of Thermophysics and Heat Transfer **3**, 203 (1989).
- [20] M. Murakami and K. Iwashita, Numerical computation of a thermal shock wave in he ii, Computers & Fluids **19**, 443 (1991).
- [21] O. C. Idowu, D. Kivotides, C. F. Barenghi, and D. C. Samuels, *Numerical Methods for Coupled Normal-Fluid and Superfluid Flows in Helium II* (Springer Berlin Heidelberg, Berlin, Heidelberg, 2001), pp. 162–176.

- [22] L. Bottura, C. Darve, N. A. Patankar, and S. W. V. Sciver, A method for the three-dimensional numerical simulation of superfluid helium, *Journal of Physics: Conference Series* **150**, 012008 (2009).
- [23] C. M.-T. Darve, Phenomenological and numerical studies of helium ii dynamics in the two-fluid model, a dissertation at the Northwestern university, Evanston, Illinois (2011).
- [24] R. A. Gingold and J. J. Monaghan, Smoothed particle hydrodynamics: theory and application to non-spherical stars, *Monthly notices of the royal astronomical society* **181**, 375 (1977).
- [25] M. Desbrun and M.-P. Gascuel, Smoothed particles: A new paradigm for animating highly deformable bodies, in *Computer Animation and Simulation96*, pp. 61–76, Springer, 1996.
- [26] M. Müller, D. Charypar, and M. Gross, Particle-based fluid simulation for interactive applications, in *Proceedings of the Eurographics symposium on Computer animation*, pp. 154–159, Eurographics Association, 2003.
- [27] J. J. Monaghan, Smoothed particle hydrodynamics, *Annual Review of Astronomy and Astrophysics* **30**, 543 (1992).
- [28] R. J. Donnelly, The two-fluid theory and second sound in liquid helium, *Phys. Today* **62**, 34 (2009).
- [29] E. LIFSHITZ and F. Leib, 12 - radiation of sound in helium iireprinted from journal of physics, 8, part 2, 110, 1944., in *Perspectives in Theoretical Physics*, pp. 177 – 183, Pergamon, Amsterdam, 1992.
- [30] I. N. Adamenko, K. E. Nemchenko, I. V. Tanatarov, and A. F. G. Wyatt, Pressure of thermal excitations in superfluid helium, *Journal of Physics: Condensed Matter* **20**, 245103 (2008).
- [31] A. Schmitt, Introduction to superfluidity, *Lect. Notes Phys* **888** (2015).
- [32] K.-H. Bennemann and J. B. Ketterson, *Novel superfluids* volume 1 (OUP Oxford, 2013).
- [33] M. Robinson, M. Ramaioli, and S. Luding, Fluid-particle flow simulations using two-way-coupled mesoscale sph-dem and validation, *International Journal of Multiphase Flow* **59**, 121 (2014).
- [34] Y. He *et al.*, A gpu-based coupled sph-dem method for particle-fluid flow with free surfaces, *Powder Technology* **338**, 548 (2018).
- [35] L. Verlet, Computer "experiments" on classical fluids. i. thermodynamical properties of lennard-jones molecules, *Phys. Rev.* **159**, 98 (1967).
- [36] J. Monaghan and A. Kocharyan, Sph simulation of multiphase flow, *Computer Physics Communications* **87**, 225 (1995), *Particle Simulation Methods*.
- [37] X. Hu and N. Adams, A multi-phase sph method for macroscopic and mesoscopic flows, *Journal of Computational Physics* **213**, 844 (2006).
- [38] A. Shakibaeinia and Y.-C. Jin, Mps mesh-free particle method for multiphase flows, *Computer Methods in Applied Mechanics and Engineering* **229-232**, 13 (2012).
- [39] C. Zhang, X. Hu, and N. Adams, A weakly compressible sph method based on a low-dissipation riemann solver, *Journal of Computational Physics* **335**, 605 (2017).
- [40] X. Xu and X.-L. Deng, An improved weakly compressible sph method for simulating free surface flows of viscous and viscoelastic fluids, *Computer Physics Communications* **201**, 43 (2016).
- [41] J. Monaghan, Simulating free surface flows with sph, *Journal of Computational Physics* **110**, 399 (1994).
- [42] Nomeritae, E. Daly, S. Grimaldi, and H. H. Bui, Explicit incompressible sph algorithm for free-surface flow modelling: A comparison with weakly compressible schemes, *Advances in Water Resources* **97**, 156 (2016).
- [43] J. Maynard, Determination of the thermodynamics of he ii from sound-velocity data, *Phys. Rev. B* **14**, 3868 (1976).
- [44] J. Wilks and D. S. Betts, An introduction to liquid helium. 2, (1987).
- [45] J. J. Monaghan, Smoothed particle hydrodynamics, *Reports on Progress in Physics* **68**, 1703 (2005).
- [46] W. F. Vinen and J. J. Niemela, Quantum turbulence, *Journal of Low Temperature Physics* **128**, 167 (2002).
- [47] K. Sasaki, N. Suzuki, D. Akamatsu, and H. Saito, Rayleigh-taylor instability and mushroom-pattern formation in a two-component bose-einstein condensate, *Phys. Rev. A* **80**, 063611 (2009).
- [48] M. S. Shadloo, A. Zainali, and M. Yildiz, Simulation of single mode rayleigh-taylor instability by sph method, *Computational Mechanics* **51**, 699 (2013).
- [49] C. Hammond, The elements, *Handbook of chemistry and physics* **81** (2000).
- [50] K. Szewc, A. Tanire, J. Pozorski, and J.-P. Minier, A study on application of smoothed particle hydrodynamics to multi-phase flows, *International Journal of Nonlinear Sciences and Numerical Simulation* **13**, 383 (2012).
- [51] C. Kirsch, *Math 529—mathematical methods for physical sciences ii*, 2011.
- [52] A. Iserles, *A First Course in the Numerical Analysis of Differential Equations* *Cambridge Texts in Applied Mathematics*, 2 ed. (Cambridge University Press, 2008).
- [53] S. Koshizuka and Y. Oka, Moving-particle semi-implicit method for fragmentation of incompressible fluid, *Nuclear science and engineering* **123**, 421 (1996).
- [54] J. Morris and J. Monaghan, A switch to reduce sph viscosity, *Journal of Computational Physics* **136**, 41 (1997).
- [55] S. Koshizuka, A. Nobe, and Y. Oka, Numerical analysis of breaking waves using the moving particle semi-implicit method, *International Journal for Numerical Methods in Fluids* **26**, 751 (1998).